Platinum-group element contents of Karelian kimberlites: implications for the PGE budget of the sub-continental lithospheric mantle

W.D. Maier

School of Earth and Ocean Sciences, Cardiff University, Cardiff CF10 3AT, UK

H. O'Brien, P. Peltonen

Geological Survey of Finland (GTK), Espoo, Finland

Sarah-Jane Barnes

Sciences de la Terre, Université du Québec à Chicoutimi, G7H 2B1, Canada

Abstract. We present high-precision isotope dilution data for Os, Ir, Ru, Pt, Pd and Re in Group I and Group II kimberlites from the Karelian craton, as well as 2 samples of the Premier Group I kimberlite pipe from the Kaapvaal craton. The samples have, on average, 1.38 ppb Pt and 1.33 ppb Pd, with Pt/Pd around unity. These PGE levels are markedly lower, by as much as 80%, than those reported previously for kimberlites from South Africa, Brazil and India, but overlap with PGE results reported recently from Canadian kimberlites. Primitive-mantle-normalised chalcophile element patterns are relatively flat from Os to Pt, but Cu, Ni and, somewhat less so, Au are enriched relative to the PGE (e.g., Cu/Pd >25.000). Pd/Ir ratios are 3,6 on average, lower than most other mantle melts. The PGE systematics can be largely explained by two components, (i) harzburgite / lherzolite detritus of the SCLM with relatively high IPGE (Os-Ir-Ru) / PPGE (Rh-Pt-Pd) ratios, and (ii) a melt component that has high PPGE/IPGE ratios. By using the concentrations of iridium in the

kimberlites as a proxy for the proportion of mantle detritus in the magma, we estimate that the analysed kimberlites contain 3-27% entrained and partially dissolved detritus from the sub-continental lithospheric mantle, consistent with previous estimates of kimberlites elsewhere (Tappe S. et al., 2016, *Chem. Geol.* http://dx.doi.org/10.1016/j.chemgeo.2016.08.019). The other major component in the samples is melt, modelled to contain an average of 0.85 ppb Pt and 1.09 ppb Pd. Assuming that Group II kimberlites are derived from relatively metasomatised SCLM, our data suggest that the metasomatised Karelian SCLM is relatively poor in Pt and Pd. If our data are representative of other Group II kimberlites elsewhere, this result could imply that the PGE enrichment in certain continental large igneous provinces, including Bushveld, is not derived from melting of metasomatised SCLM.

Keywords. Kimberlite, platinum-group elements, sub-continental lithospheric mantle, Finland, Karelian craton, Kaapvaal craton, Premier kimberlite pipe, Kaavi kimberlite

1. INTRODUCTION

Several recent workers have suggested that cratonic large igneous provinces (LIPs) are more prospective to host deposits of platinum-group elements (PGE) than off-cratonic LIPs because cratonic magmas can scavenge PGE during ascent through the sub-continental lithospheric mantle (SCLM) (Zhang et al., 2008; Griffin et al., 2013; Hughes et al., 2015). However, the global database on SCLM rocks, consisting largely of mantle xenoliths in kimberlite and basalt, indicates that the cratonic SCLM is mostly relatively Pt and Pd depleted compared to the primitive mantle (Irvine et al., 2003; Pearson et al. 2003, 2004; Wittig et al., 2010; Maier et al., 2012; Barnes et al., 2015). It could be argued that the xenoliths are not representative of the PGE content of the SCLM as the most metasomatised, potentially relatively PGE enriched, mantle components should be relatively more susceptible to entrainment, disaggregation and dissolution during mantle melting

50 and magma ascent. In order to address the question whether the SCLM can be locally enriched in
51 PGE we determined the concentrations of PGE in 9 samples of kimberlite from the Karelian craton
52 and 2 samples from the Kaapvaal craton.

53 Kimberlites are volatile-rich, potassic, ultramafic igneous rocks that are the main hard-rock
54 source of diamond. They are normally sub-divided into Group I and Group II. Group I has
55 abundant large crystals of olivine, in a matrix of olivine, monticellite, perovskite, spinel, mica,
56 calcite, and serpentine, whereas Group II typically has abundant phlogopite ± olivine in a matrix of
57 phlogopite, K-richterite, and other diagnostic minerals. Mitchell (1995) reinstated the name
58 "Orangeites", originally coined by Wagner (1928), for the Group II kimberlites. Mineralogically,
59 the orangeites are akin to olivine lamproites (except for the lack of carbonate in the latter), and it is
60 now generally agreed that orangeites are the southern African equivalents of lamproites (Mitchell,
61 2006), rather than being synonymous with Group II kimberlites in general.

62 Kimberlites are characterized by high abundances of not only the most incompatible trace
63 elements (e.g., Rb, Ba, Th, Nb, LREE, Sr), but also of compatible elements such as Mg, Ni and Cr.
64 This paradoxical duality is interpreted to reflect the mixing of incompatible element-rich kimberlite
65 "melt" with MgO-, Ni- and Cr-rich lithospheric mantle rocks, the dissolved and undissolved
66 remnants of which form the rock and mineral detritus in kimberlites known as xenoliths,
67 macrocrysts and megacrysts. In view of the mostly relatively low Pt and Pd contents of sub-
68 continental lithospheric mantle harzburgite and lherzolite sampled by nodules and massifs (average
69 around 3-5 ppb Pt, <1-3 ppb Pd; Irvine et al., 2003; Pearson et al., 2004; Becker et al., 2006; Smith
70 et al., 2009; Wittig et al., 2010; Maier et al., 2012), it is likely that, if the SCLM contained more
71 PGE-rich portions, these were more fusible and may have formed from metasomatic melts or
72 fluids. As such, they could be represented by the kimberlites, notably those of Group II for which
73 SCLM derivation is least controversial (Mitchell, 2006). In contrast, if both kimberlites and SCLM
74 derived xenoliths are PGE depleted compared to the sub-lithospheric mantle, this would lend

75 further credence to the model that the SCLM in general is relatively PGE poor.

76

77 **2. SAMPLES**

78 The Karelian Group II samples analysed here are from the 1.2 Ga Seitäperä intrusion and the
79 Lentiira dike swarm located between the villages of Kuhmo and Lentiira in eastern Finland
80 (O'Brien and Tyni, 1999; O'Brien et al., 2007), 350 km inwards from the craton margin (**Fig. 1**). The
81 most distinctive feature of these potassic, ultramafic rocks is their phlogopite-rich nature **(Fig. 2**a).
82 Phlogopite occurs rarely as macrocrysts, but it is abundant as phenocrysts and microphenocrysts
83 with relatively Ti-rich compositions similar to those of microphenocrysts in lamproites. The more
84 primitive potassic rocks may also contain large amounts of olivine macrocrysts and, in some cases,
85 abundant xenocrysts and xenoliths of mantle peridotite. Additional groundmass minerals include K-
86 richterite, Mn-rich ilmenite, Cr-rich spinel zoned to Ti-magnetite, apatite and perovskite in a calcite
87 + serpentine matrix. More evolved versions of this rock type contain abundant olivine phenocrysts,
88 low-Al clinopyroxene, and phlogopite that is zoned to low-Ti tetraferriphlogopite, similar to mica
89 zoning trends in Group II kimberlites (Mitchell, 1995). Because the rocks contain primary
90 carbonate, they are more akin to South African Group II kimberlites (orangeites) than olivine
91 lamproites or ultramafic lamprophyres. Similarly to orangeites, the Seitäperä Group II kimberlites
92 have enriched Nd isotopic signatures with εNd around -7, yet with distinct compositions of
93 $^{87}Sr/^{86}Sr_i$ around 0.704-0.706 (**Fig. 3**; Kargin et al., 2013; O'Brien, 2015).

94 The Finnish Group I kimberlite samples come from the 600 Ma old pipes of the Kaavi-Kuopio
95 kimberlite clusters that are located in a craton margin tectonic setting in eastern Finland. Samples of
96 pipes 1,2,3,5,9,10, and 14 are hypabyssal kimberlites. They all have typical Group I mineralogies
97 (i.e. abundant large rounded grains (macrocrysts) of olivine in a matrix of subhedral to euhedral
98 olivine, monticellite, perovskite, spinel, mica, apatite, calcite and serpentine), major and trace
99 element and isotopic compositions (O'Brien and Tyni, 1999). They display the classic suite of

100 lithospheric mantle-derived xenoliths and xenocrysts (**Fig. 2b),** including (i) variable amounts of
101 olivine showing a trimodal size distribution with abundant 0.1-0.4mm size grains mostly interpreted
102 as phenocrysts, 1-5 mm sized rounded macrocrysts, and occasional cm sized megacrysts. (ii) Mg-
103 ilmenite, (iii) pyrope garnet derived from a range of sources including high Cr, Ca-depleted
104 harzburgite to Ca-saturated lherzolite and Ca-rich wehrlite, to Ti-rich megacryst-compositions, and
105 orange garnets derived from mantle eclogite, (iv) clinopyroxene comprising lherzolitic, low-Cr
106 megacrystic, and eclogitic subgroups (O'Brien, 2015), and (v) spinels from upper mantle spinel
107 lherzolites and rare chromites plotting within the diamond inclusion field (O'Brien, 2015). The
108 rocks have relatively depleted isotopic signatures (Kargin et al., 2014) plotting close to South
109 African Group I kimberlites as well as kimberlites in Canada (Tappe et al., 2016) in εNd vs Sr_i,
110 albeit at slightly lower εNd (around 0) **(Fig. 3**, O'Brien and Tyni, 1999**)**.

111 In addition to the Finnish kimberlites, we also analysed two kimberlite samples from the
112 Kaapvaal craton. They represent Group I hypabyssal tuffissitic kimberlite breccias exposed in drill
113 core from the 1151 Ma (Wu et al., 2013) Premier pipe, located in the vicinity of Pretoria. The rocks
114 contain abundant large (up to 1 cm in diameter) macrocrysts and clasts of pelitic and quartzitic
115 country rocks set in a fine grained groundmass. The lithophile element composition of the rocks has
116 previously been reported in Maier et al. (2005), and geological-mineralogical data on the Premier
117 pipe can be found in Bartlett et al. (1994) and de Wit et al. (2016).

118

119 **3. ANALYTICAL METHODS**

120 All of our samples have been characterised for major and trace elements at the Geological Survey of
121 Finland in Espoo. The concentration of the lithophile elements in the Finnish samples is reported in
122 O'Brien and Tyni (1999) and that of the Premier samples in Maier et al. (2005). Preparation of the
123 Finnish kimberlite samples involved crushing of approximately 500 g of sample material into small
124 chips with a hammer and hand-picking approximately 200 g of chips least contaminated by crustal

125 xenoliths. No attempt was made to separate mantle xenoliths from kimberlite. The hand-picked
126 material was powdered in a steel grinding vessel. Major elements and S were determined by XRF
127 on fusion beads, H_2O and CO_2 by LECO analyzer, Ba, Ni, Cr, Cu, Zn, Sr and Zr by XRF on pressed
128 pellets and REE, Hf, Ta, Pb, Th, U, Nb, Y, Rb, Sc, V, and Co by ICP-MS. Analytical methods are
129 reported in O´Brien and Tyni (1999) and the data are provided in **Table 1**.

130 The PGE (Os, Ir, Ru, Rh, Pt, Pd) and Au have previously been determined by Ni-fire assay Te-
131 co-percipitation followed by ICP-MS at the Geological Survey of Finland. Details of the analytical
132 method are outlined in Juvonen et al. (2002) and the data are listed in **Electronic Appendix 1**. The
133 concentration of Pt and Pd in the kimberlites were found to be very low (mostly <2 ppb) and lower
134 than those reported in the literature for kimberlites (McDonald et al., 1995). In order to obtain better
135 precision the samples were additionally analysed by high pressure asher digestion followed by
136 online separation and quantification by isotope-dilution (HPA-ID) using ICP-MS following the
137 method of Meisel et al. (2003). Rock powder (2 g) was weighed in a 30 ml quartz HPA tube. Five
138 milliliters of 15 mol l^{-1} HNO_3 and 2 ml of 12 mol l^{-1} HCl (both environmental grade) were added
139 and variable amounts of a PGE-mixture spiked solution (UQAC-S-1) were added. The quartz lids
140 were closed with a quartz disk and a PTFE (polytetrafluoroethylene) strip prior to high-pressure
141 digestion at 300°C for 4.5 hr. The confining pressure was adjusted to 100 bars at the beginning and
142 increased to 130 bars during digestion. After digestion, the samples were transferred to a 30 ml PFA
143 container and directly sparged into the ICP-MS by bubbling argon through the sample for osmium
144 isotope ratio determination. The samples were dried at 70–80 °C and the residuum was diluted with
145 2-10 ml of 0.1 mol l^{-1} HCl. After centrifugation, 1 ml of the solution was introduced into a 1-m-long
146 cation exchanged resin column (previously washed with 6 mol l^{-1} HCl and equilibrated at 0.1 mol l^{-1}
147 HCl). The column was directly attached to the ICP-MS for ‘online’ separation. A multiple PGE-Au
148 and Re stock solution (SCP Science, Canada) was used to monitor the mass drift. The enriched

isotopes in the spike mixture are ^{99}Ru, ^{108}Pd, ^{185}Re, ^{190}Os, ^{191}Ir and ^{198}Pt while the isotopes used for quantification are ^{101}Ru, ^{106}Pd, ^{187}Re, ^{188}Os, ^{193}Ir and ^{196}Pt. Because they are monoisotopic, Rh and Au cannot be determined by isotope dilution technique. The signal detected from the acid blank (0.1 mol l^{-1} HCl) injected in the column prior to each analysis was subtracted from the raw count to the detector. When counts are present in the blank, the blank/sample proportion is far less than 1%. Because the on-line separation leads to changes in the signal intensity with time, it is difficult to convert the blank signal into an equivalent concentration, thus limits of detection can only be estimated and are ranging between 0.003-0.086 ng g^{-1} for Re and Pd, respectively (Savard et al., 2010). Indeed, as it is stated in Savard et al. (2010): "The MLD cannot readily be calculated precisely for HPA-ID because the result is obtained by a summation of the signal integrated over a period of time that can vary, and during which the signal intensity also varies". As also stressed in Meisel et al. (2003), the technique requires only concentrated acids and highly diluted HCl, thus procedural blank levels are controlled by the quality of the acid. Meisel et al. (2003) presented detection limits calculated on the absolute amount of total procedural blanks using reagent grade acids and found total procedural blanks ranging between 4 pg and 408 pg for Os and Pt, respectively. For the present work, the environmental acid grade used, in combination with a newer generation of ICP-MS instrument (Agilent 7700X) resulted in absolute procedural blanks ranging between 0.4 pg and 9.3 pg for Re and Pt, respectively (see **Table 2**). These values are lower than the detection limit (**Table 3**). More details on the method are provided in Meisel et al. (2003), Savard et al. (2010), Meisel and Moser (2004a, b) and Savard et al. (2010).

Table 3 reports results obtained for the reference materials analyzed together with the kimberlite samples to monitor quality. Results for OKUM agree with certificate values within the confidence limits. For Re and Os there are no certificate values, therefore the values obtained by Savard et al. (2010) are listed for comparison. The results for Re are similar, however the Os value is considerably higher, at 1.2 ng/g vs 0.79 ng g^{-1}. It is possible that the difference in Os values is real,

and due to inhomogeneity in the sample, given the low concentration of Os and the low sample weight used in isotope dilution. A round robin has recently been conducted on PGEs, Re and Au in OKUM in order to obtain certification of OKUM following ISO guidelines (Kane and Potts, 1997), however the report is not yet available (Thomas Meisel, personal communication). From 8 participating laboratories who provided Os concentrations using various preparation and analytical techniques (fire assay, Carius tube, isotope dilution, acid digestion, fusion, Q-ICP-MS, MC-ICP-MS), the data range from ~0.4 to ~1.6 ng g^{-1} Os, with >20% of the provided results showing values >1 ng g^{-1} Os. It was suggested that the working value for Os in OKUM after "outlier rejection" should be 0.85 +/- 0.12 ng g^{-1} Os, thus RSD is ~14% suggesting Os distribution in OKUM is inhomogeneous (Thomas Meisel, personal communication). In the present work, two aliquots of OKUM were analyzed and the relative standard deviations for Ru, Pd and Pt are < 5%. However for Os, Ir and Re the relative standard deviations are higher, ranging between 15% and 21% RSD. The higher relative standard deviations for these elements may be the result of a combination of low sample weights, low concentrations and inhomogeneous distribution of the elements in the sample. Again, results from the round robin show that RSD for Ir, Ru, Pt are around 12-13%.

4. RESULTS

The results for PGE by HPA-ID-ICP-MS analyses cover a similar range to those obtained by Ni-fire assay (**Fig. 4**). Combined Pt + Pd contents of the analysed Group I and Group II kimberlites from Finland and South Africa are generally below 5 ppb (**Table 2**). On average, the samples contain 1.38 ppb Pt and 1.33 ppb Pd (Pt/Pd ~1). There is very little difference between Group I and Group II, except that average Au contents of Group II samples are about twice those in Group I (1.19 ppb vs 0.63 ppb, respectively). There is also little difference in PGE contents between the Premier samples and the other kimberlites, a surprising result in view of the fact that Premier intruded rocks of the Bushveld Complex, the world's largest repository of PGE. Combined IPGE

contents in our kimberlite samples are between ~1 and ~4 ppb, with average values being 0.77 ppb Os, 0.51 ppb Ir, 1.22 ppb Ru, and 0.34 ppb Rh.

Most of the mantle normalised PGE patterns are moderately fractionated (Ir/Os 0.71*CI, Ir/Ru=0.64*CI, Ir/Rh=0.42*CI) (CI from McDonough and Sun, 1995), but Pd/Ir =2.18*CI and Pt/Ir =1.23*CI (Table 2). The Pd/Ir ratios are lower, and the metal patterns less fractionated, than in most other mantle derived magmas, with the exception of some komatiites and picrites (see compilations in Barnes et al., 1985; Maier and Barnes, 2004; Fiorentini et al. 2010; Day et al., 2013; Barnes et al., 2015). However, the metal patterns mostly show enrichment in Ni, Cu and Au relative to PGE on mantle normalized plots (**Fig. 4a-c**).

Our samples show markedly lower PGE contents than the kimberlites analysed by McDonald et al. (1995) who reported average concentrations of 1.45 ppb Os, 1.34 ppb Ir, 2.97 ppb Ru, 0.9 ppb Rh, 7.7 ppb Pt, 5.1 ppb Pd and 1.8 ppb Au in their Group I and Group II samples from South Africa and Brazil (**Fig. 4e-f**). Our PGE contents are also lower, by about 50%, than the results of Rao et al. (2014) for orangeites from the Bastar craton of India which showed average PGE contents of 3.5 ppb Ru, and ~3 ppb Pt and Pd each (Fig. 4g) However, our PGE levels are broadly similar to those of Tappe et al. (2016) who analysed Os, Ir, Ru, Pt, Pd and Re in two Canadian kimberlite clusters (Renard and Wemindji), using ID-N-TIMS for Os and ID- ICP-MS for the other PGE (**Fig. 4h**). It is thus possible that kimberlites have more variable PGE contents than reported by us. Alternatively, the relatively high PGE levels in the study of McDonald et al. (1995) could reflect the lower precision of the INAA method and the heterogeneity of the standard used; Tredoux and McDonald (1996) state coefficients of variation between 10 and 20% for the analysis of Pt and Pd in standard WITS-1 used by McDonald et al. (1995). Future work will undoubtedly clarify this issue.

5. DISCUSSION

5.1. Petrogenesis of platinum-group elements in kimberlites

The estimated concentrations of the PGE in the Earth's primitive mantle (PM) range from 1-7 ppb for individual elements (Palme and O'Neill, 2003; Barnes and Maier, 1999, Puchtel et al., 2004, Becker et al., 2006; Fischer-Gödde et al., 2011; Aulbach et al., 2016). Metal patterns in SCLM xenoliths show broadly similar levels on mantle normalized plots for Ni and the IPGE (Os, Ir, and Ru) at around 1 times primitive mantle, but Pt, Pd, Au and Cu tend to be variably depleted relative to the IPGE and PM (Pearson et al., 2003, 2004). This pattern is generally interpreted to be the result of extraction of basalt and komatiite from PM, with Ni and the IPGE behaving compatibly during much of the melting history due to partitioning into chromite, olivine, sulfides and alloys, whereas Pt, Pd, Au and Cu are incompatible (Barnes et al., 1985; Peach et al. 1990; Fleet et al. 1991, 1999; Sattari et al. 2002; Lorand et al., 2013; Mungall and Brenan, 2014; Aulbach et al., 2016; Brenan et al. 2016). Current estimates of the average PGE content of the SCLM suggest about 50-70% less Pt and Pd than in PM (Irvine et al., 2003; Pearson et al., 2004; Maier et al., 2012), but there is a certain degree of regional variation, with some cratons being relatively depleted compared to the global average (Greenland, Wittig et al., 2010) whereas others are slightly enriched (see compilation of data for various cratons in Maier et al., 2012). Rhodium behaves in a transitional manner, as seen by its relatively slight depletion relative to IPGE in the xenolith data (Fischer-Gödde et al., 2011; Maier et al., 2012; Barnes et al., 2015).

Assuming an average concentration of 250 ppm S in the convecting mantle (approximately 0.06% sulfide; McDonough and Sun, 2005), and a S solubility in basalt - komatiite at sub-lithospheric depth (>100-150 km) on the order of 500-1000 ppm (Mavrogenes and O'Neill, 1999), the bulk of the mantle sulfide is normally considered to be dissolved during moderate to large degree mantle melting (> 15-25%; Barnes et al., 1985; Mungall and Brenan, 2014). At lower degrees of melting, sulfide would be incompletely dissolved and thus the bulk of the highly chalcophile Pt, Pd, Au and Cu may remain in the mantle. The Pt and Pd depletion observed in the

mantle normalized patterns of mantle xenoliths therefore implies that the bulk of the SCLM is the residue of relatively large degree partial melting. Ballhaus et al. (2006) suggested that mantle sulfides can be entrained in magmas that formed at small degrees of mantle melting, but based on the low PGE contents reported here this model does not appear to apply to the kimberlites discussed in the present paper.

As few mantle SCLM xenoliths contain less than 1 ppb Pd, the SCLM appears to have been refertilized with melt or fluid that contained some Pd (Lorand et al., 2008; 2013), and this probably also introduced some Cu, Pt and Au. The precise nature and PGE content of the refertilising agent remains debated and was likely diverse (Simon et al., 2007; Kamenetsky et al., 2013), but the paucity of mantle samples that contain significantly higher Pt and Pd than PM (Pearson et al., 2004; Maier et al., 2012; Lorand et al., 2013) suggests that the agent was relatively PGE poor (but see Hughes et al. 2014 and Marchesi et al. 2014 for examples of relatively PGE rich SCLM xenoliths from the North Atlantic craton and the Rhonda peridotite massif).

Compared to most other mantle derived magmas (Fiorentini et al., 2010; Barnes et al., 2015) the kimberlites analysed in the present study have relatively unfractionated PGE patterns (but with several samples showing positive Rh anomalies) that can be modeled as a mixture of PGE-poor melt with high PPGE/IPGE ratios, and SCLM detritus (**Fig. 4**). For example, a 20% component of average SCLM (Maier et al., 2012) would result in ~ 0.7 ppb Ir, 0.8 ppb Pt, and 0.4 ppb Pd, accounting for most of the Ir in the analysed kimberlites, but only a fraction of the Pt and Pd. We can broadly replicate the measured patterns of the kimberlites, including the unique positive Rh anomalies, with a mixture of 10-20% average Kaapvaal peridotite xenoliths and 80-90% melt represented by the “liquid” component (see section 5.4 and **Electronic Appendix 2** for calculation method) of MARID xenoliths, rocks that are composed mainly of mica, amphibole, rutile, ilmenite, and diopside (Dawson and Smith, 1977). The MARIDs have been interpreted, by some authors, as mixtures between SCLM derived melts and mantle peridotite (Waters, 1987; Gregoire et al., 2002).

They contain, on average, 2.4 ppb Pt and Pd each, and have more fractionated PGE patterns than the harzburgite xenoliths, with Pd/Ir ~11 and Cu/Pd ~26000 (Maier et al., 2012). It should be noted that in addition to peridotite and MARID melt, the elevated CO_2 contents of kimberlite requires a carbonate component, possibly derived from melting of trace carbonatite in the SCLM.

The similarity in PGE patterns between Group I and Group II kimberlites seen in figure 4 is notable, being that most authors interpret the 2 types of kimberlites to be derived from different mantle sources; Group I kimberlites have Nd and Sr isotope ratios around CHUR, putatively reflecting an asthenospheric source (e.g., Tappe et al., 2012), whereas Group II kimberlites have strongly radiogenic Sr and unradiogenic Nd isotopes, arguably reflecting a lithospheric mantle dominated source (Smith, 1983; Tainton and McKenzie, 1994; Mitchell, 2006; O'Brien, 2015). One might expect that melts from such diverse mantle domains should have contrasting PGE patterns.

We suggest that the similarity in PGE patterns can be understood within the context of a model whereby the bulk of the PGEs in both types of kimberlite is derived from refractory cratonic mantle material. The metasomatised component of the SCLM was PGE poor, consistent with the low sulfide and PGE contents of MARIDs and other metasomatised harzburgite/lherzolite xenoliths (Pearson et al., 2004; Maier et al., 2012; Lorand et al., 2013). Only Group II magmas fused potassic metasomes that control the lithophile trace element isotope systems such as Rb-Sr, Sm-Nd, Lu-Hf, thereby causing the enriched isotope signatures of the Group II magmas. In both the Karelian and Kaapvaal craton the Group II kimberlites are older than the Group I kimberlites; Possibly, Group I kimberlites retained their relatively depleted isotopic signature during traverse through the SCLM because the SCLM had become relatively refractory, following melting events that may have included the one which resulted in the Group I kimberlites.

We considered whether the PGE could have been extracted from the kimberlites by sulfide or sulfate that segregated during magma ascent and contamination in the crust. The kimberlites have variable amounts of lower, middle and upper crustal material, but none of these rocks contain

299 significant sulfur. In any case, kimberlite magmas are generally believed to ascend relatively fast
300 within the crust, as suggested by the abundance of dense phases such as spinel crystals and large
301 peridotite fragments, and by the presence of diamonds which would have been amenable to burning
302 if the magma ponded or decelerated. This suggests that the ubiquitous PGE depletion of the
303 kimberlites was not caused by the segregation of small sulfide droplets from the magmas.
304
305 **5.2. Implications for the genesis of Bushveld Complex magmas**
306 The Bushveld Complex is the largest layered intrusion on Earth. The extensive granitic, rhyolitic
307 and mafic-ultramafic rocks outcropping across > 100 000 km^2 of southern Africa are the result of
308 one of the world's largest igneous events, with > 1M km^3 of magma (Rajesh et al., 2013). The
309 Complex has been interpreted as having crystallised from melts derived, at least in part, from the
310 SCLM, based on Os isotopes and high Pt/Pd ratios of 1.6 that mirror, amongst known mantle
311 reservoirs, only the SCLM (Maier and Barnes, 2004; Richardson and Shirey 2008, Barnes et al.,
312 2010). However, if our kimberlite data are representative of not just the Karelian craton, but also the
313 Kaapvaal craton, as suggested by the similarity in PGE patterns between the Karelian and Premier
314 kimberlite samples, this interpretation seems difficult to reconcile with the low PPGE contents and
315 the unfractionated PGE patterns in our samples, implying low PGE contents of the metasomatic
316 component of the SCLM, as discussed above; Bushveld melts have not only much more
317 fractionated PGE patterns than kimberlites (**Fig. 5**), but amongst the highest PGE contents of global
318 magmas, and they also lack the positive Au anomalies observed in Group II kimberlites (**Fig. 5**).
319 Furthermore, MELTS modelling indicates that partial melting of fertile SCLM at 30 kbar yields
320 magma that has significantly lower SiO_2 and CaO, and far higher incompatible lithophile trace
321 element contents than unevolved Bushveld B1 magma (Maier et al., 2016). We thus conclude that,
322 if the PGE contents of the two analysed Premier kimberlites are representative of other Kaapvaal
323 kimberlites, the PGE-rich Bushveld magmas are unlikely to be derived mainly from the

metasomatised portion of the SCLM. Alternatively, it is possible that the PGE contents of our Premier kimberlite samples are not representative of Kaapvaal kimberlites, as potentially suggested by the data of McDonald et al. (1995). However, as pointed out earlier, we feel that the INAA method used by these authors lacks the precision required to reliably determine the low abundances of PGE in kimberlites. Future studies will doubtlessly shed more light on this issue.

A further possibility is that the SCLM xenoliths so far analysed from the Kaapvaal craton are non-representative. Marchesi et al. (2014) and Hughes et al. (2014) have reported elevated PGE contents (and high Pt/Pd > 1) in the Rhonda SCLM massif and in xenoliths from the North Atlantic craton. One could thus argue that the Kaapvaal SCLM too contains domains that are more enriched in PGE than those samples by the xenoliths analysed so far, and that Bushveld magmas selectively scavenged PGE from the ~ 150 km thick refractory SCLM during ascent. Additional work on the Kaapvaal mantle rocks is required to resolve this issue. .

5.3. Origin of elevated Au contents in the Group II kimberlites

The positive Au anomalies and elevated Au contents of the Group II samples relative to Group I kimberlites could suggest that the metasomatised component of the SCLM is relatively enriched in Au. This observation is potentially consistent with studies suggesting that the Au in orogenic Au deposits is derived from alkaline magmas sourced from the lithospheric mantle (Hronsky et al., 2012). However, due to the small number of Group II samples analysed by us this model remains highly speculative and needs to be tested by analysis of further samples. Notably, a relative Au enrichment was also observed in South African orangeites relative to South African Group I kimberlites by McDonald et al. (1991).

5.4. Estimating the proportion of xenoliths, xenocrysts and primary kimberlite melt

Kimberlites contain abundant xenoliths and xenocrysts in various states of dissolution. This

is, for example, reflected in trajectories from kimberlite towards the lithospheric mantle data array in binary Ir vs Ru and , to a lesser degree, Ir vs MgO diagrams (**Fig. 6**). Previous authors have attempted to quantify the relative proportion of peridotite detritus and kimberlite liquid by using a variety of modelling approaches, including subtraction of olivine or peridotite from bulk kimberlite (Fraser and Hawkesworth, 1992; Le Roex et al., 2003; Kjarsgaard et al., 2009), mixing models of Os isotope ratios (Pearson et al., 2003; Tappe et al., 2016), Nd-Hf isotopes (Tappe et al., 2013), calculating melt composition from the composition of non-xenocrystic olivine (Arndt et al., 2010), analysis of quenched kimberlite melt (Price et al., 2000; Kopylova et al., 2007), and melt inclusions in olivine (Kamenetsky et al., 2013). With the exception of the melt inclusion work that yielded highly carbonaceous melt estimates, most of the proposed melt compositions show relatively good consistency (e.g., 20-30% SiO_2 and MgO, 1300-2400 ppm Cr, 800-1400 ppm Ni).

A potential shortcoming of the olivine-peridotite subtraction method is that kimberlites have MgO, Cr and Ni contents that differ by a factor of less than 2 from the composition of lithospheric mantle peridotites, rendering these elements relatively insensitive tracers of melt–peridotite mixing (Smith et al., 1985; Shee, 1986; Taylor et al., 1994; Berg and Carlson, 1998; Price et al., 2000, Le Roux et al. 2003, Harris et al., 2004, Becker and Le Roex, 2006).

In the present paper, we estimate the proportion of detrital material in kimberlite by using mass balance based on Ir contents. The reasoning behind this method is that Ir abundances in low-degree mantle melts and lithospheric peridotites show very different concentrations, and that Ir is mostly relatively immobile during mantle metasomatism and near surface alteration (but see Ackerman et al., 2009, and Lorand et al., 2013, for examples of Ir depleted metasomatised mantle rocks). Iridium was also chosen for more practical reasons: due to low reagent blanks and a lack of interfering ions it can be accurately determined not only by ID but also by conventional analytical techniques such as nickel sulfide fire assay followed by ICP-MS finish.

The following equations apply:

$$Ci(pkm) = \frac{[CIr(s) - f(a) \times Ci(a)]}{[1 - f(a)]} \quad (1)$$

$$f(a) = \frac{[CIr(s) - CIr(pkm)]}{[CIr(a) - CIr(pkm)]} \quad (2)$$

where *Ci* and *CIr* refer to the concentrations of an element of interest and iridium in the sample (s), the lithospheric mantle assimilant (a), and the primary kimberlite magma (pkm). *f (a)* refers to the volume fraction of the assimilant in the sample. To solve the equation for unknown elements one needs to know the composition of the assimilant and the Ir content of the primary kimberlite melt.

The composition of the assimilant is estimated by averaging the compositions of mantle xenoliths that have been recovered from kimberlite pipes. With the exception of a few pipes (notably Jagersfontein), this proved to be remarkably homogenous for the Kaapvaal and Karelian cratons, at 3.67 ppb Ir for the Kaapvaal craton (n=83, stdev 1.62ppb) and 3.62 ppb Ir for the Karelian craton (n=18; stdev 2.19, Pearson et al., 2004, Becker et al., 2006; Maier et al., 2012). Alard et al. (2000) have proposed that in cratonic peridotites Ir is mainly bound in sulfide minerals found as inclusions in olivine, but Luguet et al. (2007) showed that in the Lherz massif laurite inclusions may occur in addition to Pt-Ir-Os alloys. Although the Ir content of kimberlite thus basically is a measure of the amount of sulfide and alloy contamination, it is likely that kimberlite melt has assimilated bulk mantle peridotite, rather than selectively Ir-rich mineral phases; The latter are protected from selectively dissolving into kimberlite magma by the enclosing olivine crystals (macrocrystal olivine) which show only minor reaction with the melt. Because the Ir content of kimberlite melt is low (see below) and D_{Ir}(ol-melt) is only around 2 (e.g., Brenan et al., 2005), possible removal of some phenocrystic olivine has no significant effect on the iridium content of the melt. Furthermore, a case can be made against gravitational removal of macrocrystal olivine (ρ=3.3

g/cm^3), because kimberlites contain abundant picroilmenite, garnet, and diamond xenocrysts, all of which have higher densities than olivine. Although nugget effect is always a possibility, we are confident that the extensive degree of assimilation by the rigorously mixing kimberlite magma provides us with well homogenised kimberlite samples in which Ir can be applied as a proxy for the degree of mantle assimilation.

The Ir content of the kimberlite parental magma can be estimated from general mantle melting constraints and the Ir content of other alkaline magma types; Firstly, Ir is largely bound in mantle sulfides (Alard et al., 2000) and, to a lesser degree, in olivine (Brenan et al., 2005). Partition coefficients between sulfide and silicate melt are between 10^5 and 10^7 (Fonseca et al., 2009; Mungall and Brenan, 2014), and between olivine and silicate melt are ~2 (Brenan et al., 2005). As a result, batch melting calculations yield <0.05 ppb Ir in melts with F<5%. Secondly, the available literature data indicate that most alkaline basalts have very low iridium contents (Vogel and Keays, 1997; Rehkämper et al., 1999; Tatsumi et al., 2000; Crocket et al., 2002; Barnes et al., 2015). Concentrations range from 0.002 to 0.365 ppb with a median value of 0.06 ppb (n=33). From these estimates we conclude that it is unlikely that primary kimberlite melts contain significantly more than 0.05 ppb iridium.

Calculations using Equation (2) suggest that the volume percentage of the lithospheric mantle material in Finnish Group I and II kimberlites is between 3-22 wt.%. The two Premier samples analysed have 18-27% mantle detritus. These estimates overlap with those of Tappe et al. (2016) for Canadian kimberlites (2-30%).

Equation (1) cannot be readily applied to calculate primary major and lithophile trace element "melt" compositions for our samples. This is because for major and lithophile trace elements, potential uncertainties are much larger than in the case of PGE, as the compositional difference between the contaminant (the xenoliths) and the kimberlite melt is far smaller than for PGE, and accumulation and fractionation effects are potentially far more significant; For example, a small

amount of cumulus phlogopite in the kimberlites dramatically changes the K and Rb contents of the rock.

6. CONCLUSIONS

(i) The present study presents high-precision isotope dilution data for Os, Ir, Ru, Pt, and Pd in kimberlites. Platinum and Pd contents of the rocks are generally very low (averaging around 1.3-1.4 ppb Pt and Pd each, 2-3 ppb combined IPGE), in contrast with some previous studies that proposed up to 4-7 times higher Pt and Pd contents and 2-3 times higher IPGE contents. We propose that the differences are largely due to the inferior precision and accuracy of those previous studies conducted by using INAA. In contrast, previous studies using ICP-MS (Tappe et al., 2016) have obtained PGE levels broadly overlapping with our results.

(ii) The PGE patterns of the kimberlites can be interpreted to represent mixtures of PGE poor melt and variably dissolved SCLM xenoliths and xenocrysts. Using Ir as a proxy, we have estimated the proportion of mantle detritus in the kimberlites to be between 3 and 28%.

(iii) Our data from the Karelian craton and the Premier pipe in South Africa suggest that the metasomatised component of the SCLM is relatively PGE poor. If the 2 Premier samples are representative of the Kaapvaal craton, this would imply that the high PGE contents and Pt/Pd ratios in Bushveld magmas are not derived from melting of the metasomatised Kaapvaal SCLM, and that the prospectivity of LIPs is not controlled by the interaction of the magmas with cratonic SCLM, as proposed in some recent studies.

(iv) The Group II kimberlites have positive Au anomalies in mantle normalised diagrams suggesting that the metasomatic component of the SCLM is relatively enriched in Au compared to PGE, and that the metasomatised SCLM could have supplied noble metals for orogenic Au deposits (Hronsky et al., 2012; Griffin et al., 2013).

8. ACKNOWLEDGEMENTS

We thank Dany Savard (UQAC) for conducting the ID analyses. S Tappe, L Ackerman, an anonymous reviewer, and associate editor C Dale provided helpful reviews.

9. REFERENCES

Ackerman L., Walker R.J., Puchtel I.S., Pitcher L., Jelínek, E. and Strnad L. (2009) Effects of melt percolation on highly siderophile elements and Os isotopes in subcontinental lithospheric mantle: A study of the upper mantle profile beneath Central Europe. *Geochim. Cosmochim. Acta.* **73,** 2400−2414.

Alard O., Griffin W.L., Lorand J.P., Jackson S.E. and O'Reilly S.Y. (2000) Non-chondritic distribution of the highly siderophile elements in mantle sulfides. *Nature* **407**, 891–894.

Arndt N. T., Guitreau M., Boullier A. M., Le Roex A., Tommasi A., Cordier P. and Sobolev A. (2010) Olivine, and the origin of kimberlite. *J Petrol*. **51**, 573-602.

Aulbach, S., Mungall, J.E. and Pearson, D.G. (2016) Distribution and processing of highly siderophile elements in cratonic mantle lithosphere. *Rev. Mineralogy Geochem.* **81**, 239-304.

Balaram V., Mathur R., Banakar V.K., Hein J.R., Rao C.R.M., Rao T.G. and Dasaram B. (2006) Determination of the platinum-group elements (PGE) and gold in manganes nodule reference samples by nickel sulphide fire-assay and Te coprecipitation with ICP-MS. *Indian J. Marine Sci*, **35**, 7-16.

Ballhaus C., Bockrath C., Wohlgemuth-Ueberwasser C., Laurenz V. and Berndt J. (2006) Fractionation of the noble metals by physical processes. *Contrib. Mineral. Petrol.* **152,** 667–684.

Barnes S.-J. and Maier W.D. (1999) The fractionation of Ni, Cu and the noble metals in silicate and sulfide melts. In *Dynamic processes in magmatic ore deposits and their application in mineral exploration* (eds. R.R. Keays, C.M. Lesher, P.C. Lightfoot and C.E.G. Farrow). Geological

Association of Canada, Short Course Notes, 13.

Barnes S.-J., Maier W.D. and Curl E. (2010) Composition of the Marginal Rocks and Sills of the Rustenburg Layered Suite, Bushveld Complex, South Africa: Implications for the Formation of the Platinum-group Element Deposits. *Econ. Geol*. **105**, 1481-1511.

Barnes S.J., Mungall J.E. and Maier W.D. (2015) Platinum group elements in mantle melts and mantle samples, *Lithos* **232**, 395-417.

Barnes S.J. and Naldrett A.J. (1985) Geochemistry of the J-M (Howland) reef of the stillwater complex, Minneapolis adit area; I, sulfide chemistry and sulfide-olivine equilibrium. *Econ. Geol.* **80**, 627–645.

Bartlett P.J. (1994). Geology of the Premier diamond pipe. In *Proceedings XVth CMMI Congress* (ed. C.R. Anhaeusser), South African Institute of Mining and Metallurgy, Symposium Series, S 14-3, 201-214.

Becker H., Horan M.F., Walker R.J., Gao S., Lorand J.-P. and Rudnick, R.L. (2006) Highly siderophile element composition of the Earth's primitive mantle: constraints from new data on peridotite massifs and xenoliths. *Geochim. Cosmochim. Acta* **70**, 4528-4550.

Becker M. and Le Roex A.P. (2006) Geochemistry of South African On- and off-craton GroupI and Group II kimberlites: petrogenesis and source region evolution. *J. Petrol.* **47**, 673-703.

Brenan J.M., Bennett N.R. and Zajacz Z. (2016) Experimental results on fractionation of the highly siderophile elements (HSE) at variable pressures and temperatures during planetary and magmatic differentiation. *Rev. Mineral. Geochem.* **81,** 1–87.

Brenan J.M., McDonough W.F. and Ash R. (2005) An experimental study of the solubility and partitioning of iridium, osmium and gold between olivine and silicate melt, *EPSL*, **237**, 855-872

Coe N., Le Roex A.P., Gurney J., Pearson D.G. and Nowell G. (2008) Petrogenesis of the Swartruggens and Star Group II kimberlite dyke swarms, South Africa: constraints from whole rock geochemistry. *Contrib. Min. Petrol.* **156**, 627-652.

497 Crocket J.H. (2002) Platinum-group elements in basalts from Maui, Hawai'i: Low abundances in
498 alkali basalts: *Can. Mineralogist* **40**, 595–-609.
499 Dawson, J.B. and Smith, J.V. (1977) The MARID (mica-amphibole-rutile-ilmenite-diopside) suite
500 of xenoliths in kimberlite. *Geochim. Cosmochim. Acta* **41**, 309IN9311-310IN11323.
501 Day, J.M., Brandon, A.D. and Walker, R.J. (2016) Highly siderophile elements in Earth, Mars, the
502 Moon, and asteroids. *Rev Mineral Geochem* **81**, 161-238.
503 Day J.M.D., Pearson D.G. and Hulbert L.J. (2013). Highly siderophile element behaviour during
504 flood basalt genesis and evidence formelts fromintrusive chromitite formation in the
505 Mackenzie large igneous province. *Lithos* **182–183**, 242–258.
506 de Wit, M., Bhebhe, Z., Davidson, J., Haggerty, S.E., Hundt, P., Jacob, J., Lynn, M., Marshall, T.R.,
507 Skinner, C., Smithson, K. and Stiefenhofer, J. (2016) Overview of Diamond Resources in Africa.
508 *Episodes* **39,** 198-238.
509 Fiorentini, M.L., Barnes, S.J., Lesher, C.M., Heggie, G.J., Keays, R.R. and Burnham, O.M. (2010)
510 Platinum-group element geochemistry of mineralized and non-mineralized komatiites and
511 basalts. *Economic Geology* **105**, 795–823.
512 Fischer-Gödde M., Becker H. and Wombacher F. (2011) Rhodium, gold and other highly
513 siderophile elements in orogenic peridotites and peridotite xenoliths. *Chemical Geology* **280**,
514 365.
515 Fleet M.E., Crocket J.H., Menghua Li. and Stone W.E. (1999) Laboratory partitioning of platinum-
516 group elements (PGE) and gold with application to magmatic sulfide-PGE deposits. *Lithos* **47,**
517 127–144.
518 Fleet M.E., Stone W.E. and Crocket J.H. (1991) Partitioning of palladium, iridium and platinum
519 between sulfide liquid and basaltic melt: effect of melt composition, concentration, and oxygen
520 fugacity. *Geochim. Cosmochim. Acta* **55,** 2545−2554.
521 Fonseca R. O., Campbell I. H., O'Neill H. S. C. and Allen, C. M. (2009) Solubility of Pt in sulphide

522 mattes: implications for the genesis of PGE-rich horizons in layered intrusions. *Geochim.*
523 *Cosmochim. Acta* **73**, 5764-5777.
524 Francis R. D. (1995) Sulfide globules in mid-ocean ridge basalts (MORB), and the effect of oxygen
525 abundance in Fe-S-O liquids on the ability of those liquids to partition metals from MORB and
526 komatiite magmas. *Chem. Geol.* **85**, 199-213.
527 Fraser K.J. and Hawkesworth C.J. (1992) The petrogenesis of group 2 ultrapotassic kimberlites
528 from Finsch Mine, South Africa. *Lithos* **28**, 327–345.
529 Gregoire M., Bell D.R. and Le Roex A.P. (2002) Trace element geochemistry of phlogopite-rich
530 mafic mantle xenoliths: their classification and their relationship to phlogopite-bearing
531 peridotites and kimberlites revisited. *Contrib. Mineral. Petrol*. **142**, 603-625.
532 Griffin W.L., Begg G.C. and O'Reilly S.Y. (2013) Continental-root control on the genesis of
533 magmatic ore deposits. *Nature Geoscience* **6**, 905-910.
534 Gurney J. J. (1984) A correlation between garnets and diamonds. In *Kimberlite Occurrence and*
535 *Origin: a Basis for Conceptual Models in Exploration* (eds. J.E. Glover and P.G. Harris).
536 Geology
537 Department and University Extension, University of Western Australia, Publication 8, 143-166.
538 Harris M., Le Roex A. and Class C. (2004) Geochemistry of the Uintjiesberg kimberlite, South
539 Africa: petrogenesis of an off-craton, group I, kimberlite. *Lithos* **74**, 149–165.
540 Hronsky, J. M., Groves, D. I., Loucks, R. R. and Begg, G. C. (2012). A unified model for gold
541 mineralisation in accretionary orogens and implications for regional-scale exploration targeting
542 methods. *Mineralium Deposita* **47**, 339-358.
543 Hughes H.S.R., McDonald I., Goodenough K.M., Ciborowski T.J.R., Kerr A.C., Davies J.H.F.L.
544 and Selbyd D. (2014) Enriched lithospheric mantle keel below the Scottish margin of the North
545 Atlantic Craton: Evidence from the Palaeoproterozoic Scourie Dyke Swarm and mantle
546 xenoliths, *Precamb. Res.* **250**, 97–126.

547 Irvine G.J., Pearson D.G., Carlson R.W., Kjarsgaard B.A. and Dreibus G. (2003) Evolution of the
548 lithospheric mantle beneath northern Canada: a Re-Os isotope and platinum-group element study
549 of kimberlite derived peridotite xenoliths from Somerset Island and a comparison to the Slave
550 and Kaapvaal cratons. *Lithos* **71**, 461-488.
551 Juvonen R., Lakomaa T. and Soikkeli I. (2002) Determination of gold and platinum group elements
552 in geological samples by ICP-MS after nickel sulphide fire assay: difficulties encountered with
553 different types of geological samples. *Talanta* **58**, 595-603.
554 Kamenetsky V. S., Grütter H., Kamenetsky M. B. and Gömann, K. (2013) Parental carbonatitic melt
555 of the Koala kimberlite (Canada): Constraints from melt inclusions in olivine and Cr-spinel, and
556 groundmass carbonate. *Chem. Geol.* **353**, 96-111.
557 Kane, J. S., and Potts, P. J. (1997) ISO Guides for reference material certification and use:
558 Application to geochemical reference materials. *Geostandards Newsletter* **21(1)**, 51-58.
559 Kargin A.V., Nosova A.A., Larionova Y.O., Kononova V.A., Borisovsky S.E., Koval'chuk E.V. and
560 Griboedova I.G. (2014) Mesoproterozoic orangeites (kimberlites II) of West Karelia:
561 Mineralogy, geochemistry, and Sr-Nd isotope composition. *Petrology* **22**, 151–183.
562 Kjarsgaard B.A., Pearson D.G., Tappe S., Nowell G.M. and Dowall D.P. (2009) Geochemistry of
563 hypabyssal kimberlites from Lac de Gras, Canada: comparisons to a global database and
564 applications to the parent magma problem. *Lithos* **112**, 236–248.
565 Kopylova M.G., Matveev S. and Raudsepp M. (2007) Searching for parental kimberlite melt.
566 *Geochim. Cosmochim. Acta* **71**, 3616–3629.
567 Le Roex A.P., Bell D.R. and Davis P. (2003) Petrogenesis of Group I kimberlites from Kimberley,
568 South Africa: Evidence from bulk-rock geochemistry. *J. Petrol.* **44**, 2261-2286.
569 Lorand J-P., Alard O. and Godard M. (2008) Platinum-group element signature of the primitive
570 mantle rejuvenated by melt-rock reactions: evidence form Sumail peridotities (Oman ophiolite).
571 *Terra Nova* **21**, 35-40.

572 Lorand J-P., Luguet A. and Alard O. (2013) Platinum-group elements systematics and petrogenetic
573 processing of the continental upper mantle: a review. *Lithos* **164−167,** 2−21
574 Luguet A., Shirey S., Lorand J-P., Horan M. and Carlson R.W. (2007) Residual platinum group
575 minerals from highly depleted harzburgites of the Lherz massif (France) and their role in HSE
576 fractionation of the mantle. *Geochim. Cosmochim. Acta* **71,** 3082−3097.
577 Luth, R.W., (2009) The activity of silica in kimberlites, revisited. *Contrib. Mineral. Petrol.* **158**,
578 283-294.
579 Maier W.D. and Barnes S.-J. (2004) Pt/Pd and Pd/Ir ratios in mantle-derived magmas: a possible
580 role for mantle metasomatism. *S. Afr. J. Geol.* **107**, 333-340.
581 Maier W.D., Peltonen P., Juvonen R. and Pienaar C. (2005) Platinum-group elements in peridotite
582 xenoliths and kimberlite from the Premier kimberlite pipe, South Africa. *S. Afr. J. Geol*. **108**,
583 413–428.
584 Maier W.D., Peltonen P., McDonald I., Barnes S.J., Barnes S.-J., Hatton C. and Viljoen F. (2012)
585 The concentration of platinum-group elements and gold in southern African and Karelian
586 kimberlite-hosted mantle xenoliths: Implications for the noble metal content of the Earth's
587 mantle. *Chem. Geol.* **302–303**, 119–135.
588 Marchesi, C., Dale, C.W., Garrido, C.J., Pearson, D.G., Bosch, D., Bodinier, J.L., Gervilla, F. and
589 Hidas, K. (2014) Fractionation of highly siderophile elements in refertilized mantle: Implications
590 for the Os isotope composition of basalts. *Earth Planet. Sci. Lett*. **400**, 33-44.
591 Meisel T., Fellner N. and Moser J. (2003) A simple procedure for the determination of platinum
592 group elements and rhenium (Ru, Rh, Pd, Re, Os, Ir and Pt) using ID-ICP-MS with an
593 inexpensive on-line matrix separation in geological and environmental materials. *J. Analytical*
594 *Atomic Spectrometry*, **18**, 720–726.
595 Meisel T. and Moser J. (2004a) Reference materials for geochemical PGE analysis: new analytical
596 data for Ru, Rh, Pd, Os, Ir, Pt and Re by isotope dilution ICP-MS in 11 geological reference

materials. *Chemical Geology* **208**, 319–338.

Meisel T. and Moser J. (2004b) Platinum-group element and rhenium concentrations in low abundance reference materials. *Geostand. Geoanal. Res*. **28**, 233–250.

McDonald I., De Wit M.J., Smith C.B., Bizzi L.A. and Viljoen K.S. (1995) The geochemistry of the platinum-group elements in Brazilian and southern African kimberlites. *Geochim. Cosmochim. Acta* **59**, 2883-2903.

McDonough, W.F. and Sun, S.-S. (1995) The composition of the Earth. *Chem. Geol.* **120**, 223–253.

Mitchell R.H. (1995) Kimberlites, orangeites, and related rocks: New York, Plenum Press, 410 p.

Mitchell, R.H. (2006) Potassic magmas derived from metasomatized lithospheric mantle: Nomenclature and relevance to exploration for diamond-bearing rocks. *J. Geol. Soc. India* **67,** 317-327.

Mungall J.E. and Brenan J.M. (2014) Partitioning of platinum-group elements and Au between sulfide liquid and basalt and the origins of mantle–crust fractionation of the chalcophile elements. *Geochim. Cosmochim. Acta* **125**, 265–289.

O'Brien H. (2015) Deposits related to carbonatites and kimberlites. In *Mineral Deposits of Finland* (eds. W.D. Maier, R. Lahtinen. and H. O'Brien), Elsevier, 792pp.

O'Brien H., Phillips D. and Spencer R. (2007) Isotopic ages of Lentiira – Kuhmo – Kostomuksha olivine lamproite - Group II kimberlites. *Bull. Geol. Soc. Finland* **79**, 203–215.

O'Brien H.E. and Tyni M. (1999) Mineralogy and geochemistry of kimberlites and related rocks from Finland: Isotopic ages of Lentiira – Kuhmo – Kostomuksha Olivine Lamproite - Group II kimberlites. In *Proceedings of the 7th International Kimberlite Conference* (ed. J.J. Gurney et al.), Cape Town, South Africa, pp. 625–636.

Palme H. and O'Neill H.St.C. (2003) Cosmochemical Estimates of Mantle Composition, In *Treatise on Geochemistry Vol. 2* (ed. R.W. Carlson). Elsevier, Amsterdam. pp. 1-38.

622 Peach C.L., Mathez E.A. and Keays R.R. (1990) Sulfide melt—silicate melt distribution
623 coefficients for noble metals and other chalcophile elements as deduced from
624 MORB:implications for partial melting. *Geochim. Cosmochim. Acta* **54,** 3379–3389.
625 Pearson D.G., Canil D. and Shirey S.B. (2003) Mantle samples included in volcanic rocks:
626 xenoliths and diamonds. In *Treatise on Geochemistry Vol. 2* (ed. R.W. Carlson). Elsevier,
627 Amsterdam. pp. 171–275.
628 Pearson D.G., Irvine G.J., Ionov D.A., Boyd F.R. and Dreibus G.E. (2004) Re-Os isotope
629 systematics and platinum-group element fractionation during mantle melt extraction: a study of
630 massif and xenolith peridotite suites. *Chem. Geol*. **208**, 29-59.
631 Peltonen, P. and Brügmann, G. (2006) Origin of layered continental mantle (Karelian craton,
632 Finland): geochemical and Re–Os isotope constraints. *Lithos* **89**, 405-423.
633 Pilbeam, L.H., Nielsen, T.F.D. and Waight, T.E. (2013). Digestion fractional crystallization (DFC):
634 an important process in the genesis of kimberlites. Evidence from olivine in the Majuagaa
635 kimberlite, southern West Greenland. *J. Petrol.* **54,** 1399-1425.
636 Price S.E., Russell J.K. and Kopylova M.G. (2000) Primitive magma from the Jericho Pipe, N.W.T.,
637 Canada: Constraints on primary kimberlite melt chemistry: *J. Petrol.* **41**, 789-808.
638 Puchtel I.S., Humayun M., Campbell A.J., Sproule R.A. and Lesher C.M. (2004) Platinum group
639 element geochemistry of komatiites from the Alexo and Pyke Hill areas, Ontario, Canada.
640 *Geochim. Cosmochim. Acta* **68**, 1361-1383.
641 Rajesh H.M., Chisonga B.C., Shindo K., Beukes N.J. and Armstrong R.A. (2013) Petrographic,
642 geochemical and SHRIMP U–Pb titanite age characterization of the Thabazimbi mafic sills:
643 Extended time frame and a unifying petrogenetic model for the Bushveld Large Igneous
644 Province. *Precamb. Res.* **230**, 79-102.
645 Rao N.V.C., Lehmann B. and Balaram V. (2014) Platinum-group element (PGE) geochemistry of
646 Deccan orangeites, Bastar craton, central India: implication for a non-terrestrial origin for

iridium enrichment at the K– Pg boundary. *J. Asian Earth Sci.* **84**, 24–33.

Rehkämper M., Halliday A.N., Fitton J.G., Lee D.C., Wieneke M. and Arndt N.T. (1999) Ir, Ru, Pt, and Pd in basalts and komatiites: New constraints for the geochemical behaviour of the platinum-group elements in the mantle: *Geochim. Cosmochim. Acta* **63**, 3915–3934.

Richardson S.H. and Shirey S.B. (2008) Continental mantle signature of Bushveld magmas and coeval diamonds. *Nature* **453**, 910–913.

Ringwood A.E., Kesson S.E., Hibberson W. and Ware N. (1992) Origin of kimberlites and related magmas. *Earth Planet. Sci. Lett*. **113**, 521-538.

Sattari P., Brenan J.M., Horn I. and McDonough W.F. (2002) Experimental Constraints on the sulfide- and chromitesilicate melt partitioning behavior of rhenium and platinum-group-elements. *Econ. Geol.* **97,** 385−398.

Savard D., Barnes S-J. and Meisel T. (2010) Comparison between Nickel-Sulfur Fire Assay Te Co-precipitation and Isotope Dilution with High-Pressure Asher Acid Digestion for the Determination of Platinum-Group Elements, Rhenium and Gold. *Geostand. Geoanalyt. Res*. **34**, 281-291.

Simon N.S.C., Carlson R.W., Pearson D.G. and Davies, G.R. (2007) The origin and evolution of the Kaapvaal cratonic lithospheric mantle. *J. Petrol.* **48**, 589–625.

Smith, C.B., Pearson, D.G., Bulanova, G.P., Beard, A.D., Carlson, R.W., Wittig, N., Sims, K., Chimuka, L. and Muchemwa, E. (2009). Extremely depleted lithospheric mantle and diamonds beneath the southern Zimbabwe craton. *Lithos* **112S**, 1120–1132.

Sobolev N. V. (1977) Deep-seated Inclusions in Kimberlites and the Problem of the Composition of the Upper Mantle. Washington, DC: American Geophysical Union.

Tainton K.M. and McKenzie D. (1994) The Generation of Kimberlites, Lamproites, and their Source Rocks, *J. Petrol.* **35,** 787-817.

Tappe S., Brand N.B., Stracke A., van Acken D., Liu C.Z., Strauss H., Wu F.Y., Luguet A. and

672 Mitchell R.H. (2016) Plates or plumes in the origin of kimberlites: U/Pb perovskite and Sr-Nd-
673 Hf-Os-CO isotope constraints from the Superior craton (Canada). *Chem. Geol.*
674 http://dx.doi.org/10.1016/j.chemgeo.2016.08.019, 27 pages
675 Tappe S., Pearson D.G., Kjarsgaard B.A., Nowell G.M. and Dowall D. (2013) Mantle transition
676 zone input to kimberlite magmatism near a subduction zone: origin of anomalous Nd-Hf isotope
677 systematics at Lac de Gras, Canada. *Earth Planet. Sci. Lett.* **371- 372**, 235–251.
678 Tappe S., Steenfelt A. and Nielsen T.F.N. (2012) Asthenospheric source of Neoproterozoic and
679 Mesozoic kimberlites from the North Atlantic craton, West Greenland: new high-precision U-Pb
680 and Sr-Nd isotope data on perovskite. *Chem. Geol.* **320-321**, 113–127.
681 Tatsumi Y., Oguri K., Shimoda G., Kogiso T. and Barsczus H.G. (2000) Contrasting behaviour of
682 noble-metal enrichments during magmatic differentiation in basalts from the Cook Islands,
683 Polynesia. *Geology* **28**, 131-134.
684 Tredoux M. and McDonald, I. (1996) Komatiite WITS-1, low concenytration noble metal standard
685 for the analysis of non-mineralized samples. *Geostandards Newsletter* **20(2)**, 267-276.
686 .Vogel D.C. and Keays R.R. (1997) The petrogenesis and platinum-group element geochemistry of
687 the Newer Volcanic Province, Victoria, Australia. *Chem. Geol*. **136**, 181-204.
688 Wagner, P.A. (1928) The evidence of the kimberlite pipes on the constitution of the outer part of the
689 Earth. *S. Afr. J. Sci*. **25**, 127–148.
690 Waters F. (1987) A suggested origin of MARID xenoliths in kimberlites by high pressure
691 crystallization of an ultrapotassic rock such as lamproite. *Contrib. Mineral. Petrol*. **95**, 523-533.
692 Wilde A., Edwards A. and Yakubchek A. (2003) Unconventional deposits of Pt and Pd: a review
693 with implications for exploration. *SEG Newsletter* **52**, p1 and 10-18
694 Wittig N., Webb M., Pearson D.G., Dale C.W., Ottley C.J., Hutchison M., Jensen S.M. and Luguet
695 A. (2010) Formation of the North Atlantic craton: timing and mechanisms constrained from Re-
696 Os isotope and PGE data of peridotite xenoliths from SW Greenland. *Chem. Geol*. **276**, 166-187.

Wu F., Mitchell R.G., Li Q., Sun J., Liu C. and Yang Y-H. (2013) In situ U-Pb age determination and Sr-Nd isotope analysis of perovskite from the Premier (Cullinan) kimberlite, South Africa. *Chem. Geol.* **353,** 83-95.

Zhang M., O'Reilly S.Y., Wang K.-L., Hronsky J. and Griffin W.L. (2008) Flood basalts and metallogeny: The lithospheric mantle connection. *Earth Sci. Rev.* **86**, 145–174.

Figure Captions

Fig. 1: Simplified geological map, showing locality of Finnish kimberlites analysed. Figure modified after Peltonen and Brügmann, (2006).

Fig. 2 (a) Phlogopite-rich group II kimberlite from dyke 16, Lentiira. Pool of late stage liquid in centre of photomicrograph is surrounded by phlogopite, tetraferriphlogopite, diopside, K-richterite. On right side of section are olivine pseudomorphs rimmed by perovskite. Plane polarised light. Modified after O'Brien and Tyni, 1995. (b) Thin section of hypabyssal kimberlite from Pipe 9 with abundant macro- and phenocrysts of olivine, as well as a fresh garnet lherzolite xenolith, containing olivine, orthopyroxene, red to purple pyrope, gray Mg-ilmenite, and bright green Cr-diopside. Plane polarized light. (c) Backscattered electron image of a Pipe 1 sample from Kaavi, Finland. Rounded olivine (bright green) is mostly altered in this sample, and all cases has a necklace of monticellite (red). Oxides are chromites (euhedral white) or late MUM spinel (skeletal small crystals, white to light yellow). Matrix is composed of serpentine (dk green), calcite (brown), kinoshitalite mica blades (yellow-orange) and euhedral apatite crystals (dark orange).

Fig. 3: Nd and Sr isotopic characteristics of Finnish kimberlites, compared to kimberlites and other alkaline rocks globally (modified after O'Brien, 2015). Data for Superior kimberlites are from

722 Tappe et al. (2016)

723

724 Fig. 4. PGE patterns of kimberlites, normalized to primitive mantle (normalization factors from
725 Becker et al. (2005) and Day et al. 2016). Data is best modelled by mixing of 10-20% SCLM and
726 80-90% MARID. Note that MARID data are normalised to mantle detritus-free composition, as
727 outlined in chapter 5.3.

728

729 Fig. 5: PGE patterns of Bushveld B1 sills (data from Barnes et al., 2010). Patterns of Premier
730 kimberlites (ID and Ni-sulfide analyses) shown in grey. Normalization factors from Becker et al.
731 (2005) and Day et al. (2016).

732

733 Fig. 6: Binary variation diagrams comparing composition of analysed kimberlites with Kaapvaal
734 and Karelian mantle xenoliths. Also plotted are diamond-bearing (Renard) and barren kimberlites
735 (Wemindji) from the Superior craton, Canada (Tappe et al., 2016). (A) Ru vs Ir, (B) MgO vs Ir.
736 Most Karelian and Kaapvaal kimberlites plot near tielines between probable kimberlite melt and
737 average Karelian SCLM (from Maier et al., 2012), suggesting that the main contaminant is garnet
738 peridotite. In contrast, Superior kimberlites are more MgO rich, possibly suggesting more dunitic
739 SCLM contaminants. Estimate of kimberlite melt is based on Price et al. (2000).

740

741

742

743

Table 1: Whole rock data for Karelian and Kaapvaal kimberlites

Sample	KAI D21	16-002 26.95	16-002 23.83	9729 5621	9729 5611	9729 5596	9729 5603	9729 5599	9729 5604	P10	P11
Craton	Karelia	Karelia	Karelia	Karelia	Karelia	Karelia	Karelia	Karelia	Karelia	Kaapvaal	Kaapvaal
craton loc	margin	margin	margin	margin	margin	margin	margin	margin	margin	centre	centre

pipe/dyke		d 16	d 16	p 10	p 14	p 2	p 5	p 3	p 9	Premier	Premier
Group	II	II	II	I	I	I	I	I	I	I	I
SiO_2 (wt%)	23.44	42.95	36.07	35.28	34.96	32.08	35.99	29.69	39.43	39.81	37.72
TiO_2	1.99	3.24	2.41	2.39	2.84	2.34	1.31	2.29	1.95	1.96	2.00
Al_2O_3	3.14	4.01	2.30	5.02	3.48	5.43	2.74	4.88	3.62	2.11	2.46
Fe_2O_3	7.97	9.93	9.79	9.59	11.49	11.79	9.47	11.29	9.32	9.36	9.63
MnO	0.28	0.14	0.15	0.19	0.19	0.26	0.17	0.35	0.15	0.14	0.15
MgO	15.02	21.68	29.47	24.19	29.96	22.58	28.39	20.89	26.95	27.31	27.06
CaO	22.48	5.44	4.87	8.30	3.78	10.09	7.27	12.59	6.19	7.16	8.24
Na_2O	dl	0.40	dl	0.21	0.14	0.10	0.14	0.11	1.05	0.06	0.01
K_2O	0.76	5.73	2.31	1.57	2.27	1.95	0.31	0.63	2.44	1.04	1.07
P_2O_5	0.87	0.12	0.39	0.58	0.34	0.60	0.27	0.69	0.34	0.33	0.42
H_2O^+	na	na	na	10.14	9.68	8.96	10.50	10.50	9.36	na	na
LOI	na	na	na	na	na	na	na	na	na	8.96	9.43
C	na	na	na	0.74	0.47	1.01	1.27	1.90	0.10	na	na
Total	75.95	93.64	87.76	98.20	99.60	97.19	97.83	95.81	100.90	98.24	98.19
Zr (ppm)	217	319	149	103	63.7	94.4	52.8	96.6	69.1	80	80
Sr	1183	467	681	776	457	890	477	889	484	441	532
Co	na	80.8	85.7	62.8	78.2	59.9	80.5	52.7	67.8	88	84
Cr	750	1238	905	1146	1334	1171	1810	1011	1339	1385	1428
Ni	471	1166	1419	840	1027	599	1266	487	986	1305	1212
V	243	65.2	78.8	118	155	173	114	170	107	99	106
Cu	38	58	60	105	119	119	80	128	77	33	50
Sc	28	14.4	8.5	17	16.8	20.5	15.1	19.3	11.2	9.96	10.2
Rb	52	187	98	99.3	86.2	100	22.9	68.3	106	92	99
Y	20	10.7	13.1	13.4	9.15	13.8	7.99	14	8.81	10	12
Nb	217	176	168	176	177	202	98.8	219	126	95.1	93.4
Ba	968	1254	1702	1971	1254	1523	627	1344	1164	1029	979
La	240	150	188	140	100	141	65	142	71.9	43	42
Ce	445	278	324	228	171	237	109	239	119	79	77
Pr	na	29.1	33	22.2	17.3	23.5	11.1	23.6	12.5	8.2	8.1
Nd	na	89.6	105	69.9	53.4	76.1	36.3	77.9	38.5	31	31
Sm	na	9.92	12.7	9	6.66	9.45	4.54	9.72	4.81	4.48	4.66
Eu	na	2.29	2.83	2.03	1.6	2.16	1.17	2.18	1.04	1.24	1.21
Gd	na	7.26	8.4	6.37	4.95	6.37	3.48	6.31	3.79	3.23	3.15
Tb	na	0.79	0.94	0.75	0.54	0.74	0.42	0.79	0.45	0.37	0.38
Dy	na	2.57	3.42	2.87	2.01	2.89	1.72	3.01	1.76	1.69	1.81
Ho	na	0.43	0.5	0.46	0.34	0.47	0.3	0.48	0.3	0.26	0.29
Er	na	0.86	0.97	1.15	0.72	1.15	0.72	1.3	0.77	0.63	0.68
Tm	na	0.09	0.11	0.13	0.09	0.17	0.09	0.16	0.09	0.074	0.081
Yb	na	0.47	0.69	0.8	0.58	0.92	0.58	0.9	0.67	0.43	0.48
Lu	na	< 0.10	< 0.10	0.11	0.1	0.13	0.1	0.13	0.11	0.06	0.064
Hf	na	9.15	4.66	2.53	2.07	2.3	1.47	2.46	1.9	1.72	1.73
Ta	na	9.52	10.1	10.2	12	11.4	6.07	11.1	8.57	6.64	6.5

Pb	na	11.4	14.3	10.9	8.62	7.82	2.41	7.46	8.24	3.37	3.77
Th	19	18	15.2	18.3	16.4	19.2	9.1	19.1	10.4	6.71	6.57
U	4	3.58	1.55	3.58	2.79	3.92	1.98	3.69	2.43	1.24	1.34
S	300	1000	2500	100	600	400	800	600	200	280	<20
Cl	na	na	na	170	500	190	150	220	280	na	na
Zn	na	na	na	87	78	84	63	89	67	52	49
Re (ppb)[1]	0.03	0.27	0.07	0.12	0.54	0.96	0.40	0.23	0.15	0.10	0.17
Os[1]	0.30	0.86	1.09	1.02	0.81	0.37	1.09	0.95	0.51	0.77	0.69
Ir[1]	0.33	0.48	0.59	0.83	0.54	0.38	0.37	0.15	0.20	0.70	1.00
Ru[1]	0.77	1.86	1.39	1.34	1.42	0.28	0.99	0.29	0.45	1.88	2.80
Rh[2]	0.15	0.28	1.24	0.18	0.33	0.08	0.43	0.13	0.21	0.35	0.39
Pt[1]	0.41	1.38	1.28	1.43	1.43	1.33	1.72	1.15	1.05	1.96	1.99
Pd[1]	0.26	1.31	1.49	1.67	0.69	1.39	3.14	1.78	0.72	1.20	0.98
Au[2]	0.70	1.04	1.84	0.26	0.48	0.68	0.75	0.66	0.94	0.43	0.47
Pd/Ir	0.80	2.74	2.55	2.01	1.28	3.66	8.42	11.87	3.67	1.72	0.98
Ir/Os	1.08	0.56	0.54	0.81	0.67	1.03	0.34	0.16	0.38	0.91	1.45
Ir/Ru	0.42	0.26	0.42	0.62	0.38	1.36	0.38	0.52	0.44	0.37	0.36
Ir/Rh	2.18	1.71	0.47	4.61	1.64	4.75	0.87	1.15	0.93	2.00	2.57
Pt/Ir	1.26	2.88	2.19	1.72	2.65	3.50	4.61	7.67	5.36	2.80	1.99

[1] HPA+ID+ICP-MS

[2] FA+ICP-MS

dl= value below detection limit; na=not analysed

744

745

Table 2: Absolute amount of total procedural blanks (in picograms) for HPA-ID procedure (n=12)

	Ru	Pd	Re	Os	Ir	Pt
Average	0.24	0.66	0.11	0.49	0.11	3.16
Stdev	0.3	0.51	0.1	0.47	0.15	2.05
Lod (X + 3s)	1.14	2.2	0.42	1.91	0.55	9.32

746

747

748

Table 3: Comparison of Results Obtained for Reference Materials by Isotope Dilution Analyses at UQAC with Certificate Values

	OKUM				LK-NIP				LLD
	UQAC		Geolabs		UQAC	Geolabs	UQAC	UQAC	UQAC
	This run n=2	stdev	Certificate	stdev	This run n=1	Certificate +	working value	stdev n=3	
Ru ppb	4.72	0.15	4.25	0.3	0.58	0.44	0.48	0.015	0.021

Pd ppb	11.29	0.07	11.70	0.5	17.03	17.96	17.08	0.15	0.086
Re ppb	0.57	0.12	*0.566	0.04	0.79	n.d.	n.d.	n.d.	0.003
Os ppb	1.20	0.18	*0.79		0.51	n.d.	n.d.	n.d.	0.044
Ir ppb	1.11	0.23	0.99	0.07	0.16	0.19	0.15	0.02	0.004
Pt ppb	11.33	0.42	11.00	0.55	13.91	13.43	12.34	0.38	0.026

OKUM = Abtibi komatiite; LK-NIP = Niping Diabase both supplied by Geolabs, Ontario; n.d. not determined; *for OKUM no certificate values are available for Os and Re so values from, Savard et al. (2010) are presented. +For LK-NIP no standard deviations were given on the certificate so in addition to certicate valuse working values and standard deviations obtained at UQAC by Ni-FA-ICP-MS are presented for comparison; # Lower limit of detection for HPA-ID-ICP-MS analysis Savard et al. (2010)

749

Table 1

Table 1: Whole rock data for Karelian and Kaapvaal kimberlites

Sample	KAI D21	16-002	16-002	9729	9729	9729	9729	9729	9729	P10
		26.95	23.83	5621	5611	5596	5603	5599	5604	
Craton	Karelia	Karelia	Karelia	Karelia	Karelia	Karelia	Karelia	Karelia	Karelia	Kaapvaal
craton loc	margin	margin	margin	margin	margin	margin	margin	margin	margin	centre
pipe/dyke		d 16	d 16	p 10	p 14	p 2	p 5	p 3	p 9	Premier
Group	II	II	II	I	I	I	I	I	I	I
SiO_2 (wt%)	23.44	42.95	36.07	35.28	34.96	32.08	35.99	29.69	39.43	39.81
TiO_2	1.99	3.24	2.41	2.39	2.84	2.34	1.31	2.29	1.95	1.96
Al_2O_3	3.14	4.01	2.30	5.02	3.48	5.43	2.74	4.88	3.62	2.11
Fe_2O_3	7.97	9.93	9.79	9.59	11.49	11.79	9.47	11.29	9.32	9.36
MnO	0.28	0.14	0.15	0.19	0.19	0.26	0.17	0.35	0.15	0.14
MgO	15.02	21.68	29.47	24.19	29.96	22.58	28.39	20.89	26.95	27.31
CaO	22.48	5.44	4.87	8.30	3.78	10.09	7.27	12.59	6.19	7.16
Na_2O	dl	0.40	dl	0.21	0.14	0.10	0.14	0.11	1.05	0.06
K_2O	0.76	5.73	2.31	1.57	2.27	1.95	0.31	0.63	2.44	1.04
P_2O_5	0.87	0.12	0.39	0.58	0.34	0.60	0.27	0.69	0.34	0.33
H_2O^+	na	na	na	10.14	9.68	8.96	10.50	10.50	9.36	na
LOI	na	na	na	na	na	na	na	na	na	8.96
C	na	na	na	0.74	0.47	1.01	1.27	1.90	0.10	na
Total	75.95	93.64	87.76	98.20	99.60	97.19	97.83	95.81	100.90	98.24
Zr (ppm)	217	319	149	103	63.7	94.4	52.8	96.6	69.1	80
Sr	1183	467	681	776	457	890	477	889	484	441
Co	na	80.8	85.7	62.8	78.2	59.9	80.5	52.7	67.8	88
Cr	750	1238	905	1146	1334	1171	1810	1011	1339	1385
Ni	471	1166	1419	840	1027	599	1266	487	986	1305
V	243	65.2	78.8	118	155	173	114	170	107	99
Cu	38	58	60	105	119	119	80	128	77	33
Sc	28	14.4	8.5	17	16.8	20.5	15.1	19.3	11.2	9.96
Rb	52	187	98	99.3	86.2	100	22.9	68.3	106	92
Y	20	10.7	13.1	13.4	9.15	13.8	7.99	14	8.81	10
Nb	217	176	168	176	177	202	98.8	219	126	95.1
Ba	968	1254	1702	1971	1254	1523	627	1344	1164	1029
La	240	150	188	140	100	141	65	142	71.9	43
Ce	445	278	324	228	171	237	109	239	119	79
Pr	na	29.1	33	22.2	17.3	23.5	11.1	23.6	12.5	8.2
Nd	na	89.6	105	69.9	53.4	76.1	36.3	77.9	38.5	31
Sm	na	9.92	12.7	9	6.66	9.45	4.54	9.72	4.81	4.48
Eu	na	2.29	2.83	2.03	1.6	2.16	1.17	2.18	1.04	1.24
Gd	na	7.26	8.4	6.37	4.95	6.37	3.48	6.31	3.79	3.23
Tb	na	0.79	0.94	0.75	0.54	0.74	0.42	0.79	0.45	0.37
Dy	na	2.57	3.42	2.87	2.01	2.89	1.72	3.01	1.76	1.69
Ho	na	0.43	0.5	0.46	0.34	0.47	0.3	0.48	0.3	0.26
Er	na	0.86	0.97	1.15	0.72	1.15	0.72	1.3	0.77	0.63
Tm	na	0.09	0.11	0.13	0.09	0.17	0.09	0.16	0.09	0.074
Yb	na	0.47	0.69	0.8	0.58	0.92	0.58	0.9	0.67	0.43

Table 2

Table 2: Absolute amount of total procedural blanks (in picograms) for HPA-ID procedure (n=12)

	Ru	Pd	Re	Os	Ir	Pt
Average	0.24	0.66	0.11	0.49	0.11	3.16
Stdev	0.3	0.51	0.1	0.47	0.15	2.05
Lod (X + 3s)	1.14	2.2	0.42	1.91	0.55	9.32

Table 3

Table 3: Comparison of Results Obtained for Reference Materials by Isotope Dilution Analyses at UQAC Certificate Values

	OKUM				LK-NIP			
	UQAC		Geolabs		UQAC	Geolabs	UQAC	UQAC
	This run n=2	stdev	Certificate	stdev	This run n=1	Certificate +	working value	stdev n=3
Ru ppb	4.72	0.15	4.25	0.3	0.58	0.44	0.48	0.015
Pd ppb	11.29	0.07	11.70	0.5	17.03	17.96	17.08	0.15
Re ppb	0.57	0.12	*0.566	0.04	0.79	n.d.	n.d.	n.d.
Os ppb	1.20	0.18	*0.79		0.51	n.d.	n.d.	n.d.
Ir ppb	1.11	0.23	0.99	0.07	0.16	0.19	0.15	0.02
Pt ppb	11.33	0.42	11.00	0.55	13.91	13.43	12.34	0.38

OKUM = Abtibi komatiite; LK-NIP = Niping Diabase both supplied by Geolabs, Ontario; n.d. not determined; *for OKUM no certificate values are available for Os and Re so values from, Savard et al. (2010) are presented. +For LK-NIP no standard deviations were given on the certificate so in addition to certicate valuse working values and standard deviations obtained at UQAC by Ni-FA-ICP-MS are presented for comparison; # Lower limit of detection for HPA-ID-ICP-MS analysis Savard et al. (2010)

Figure 1

Click here to download high resolution image

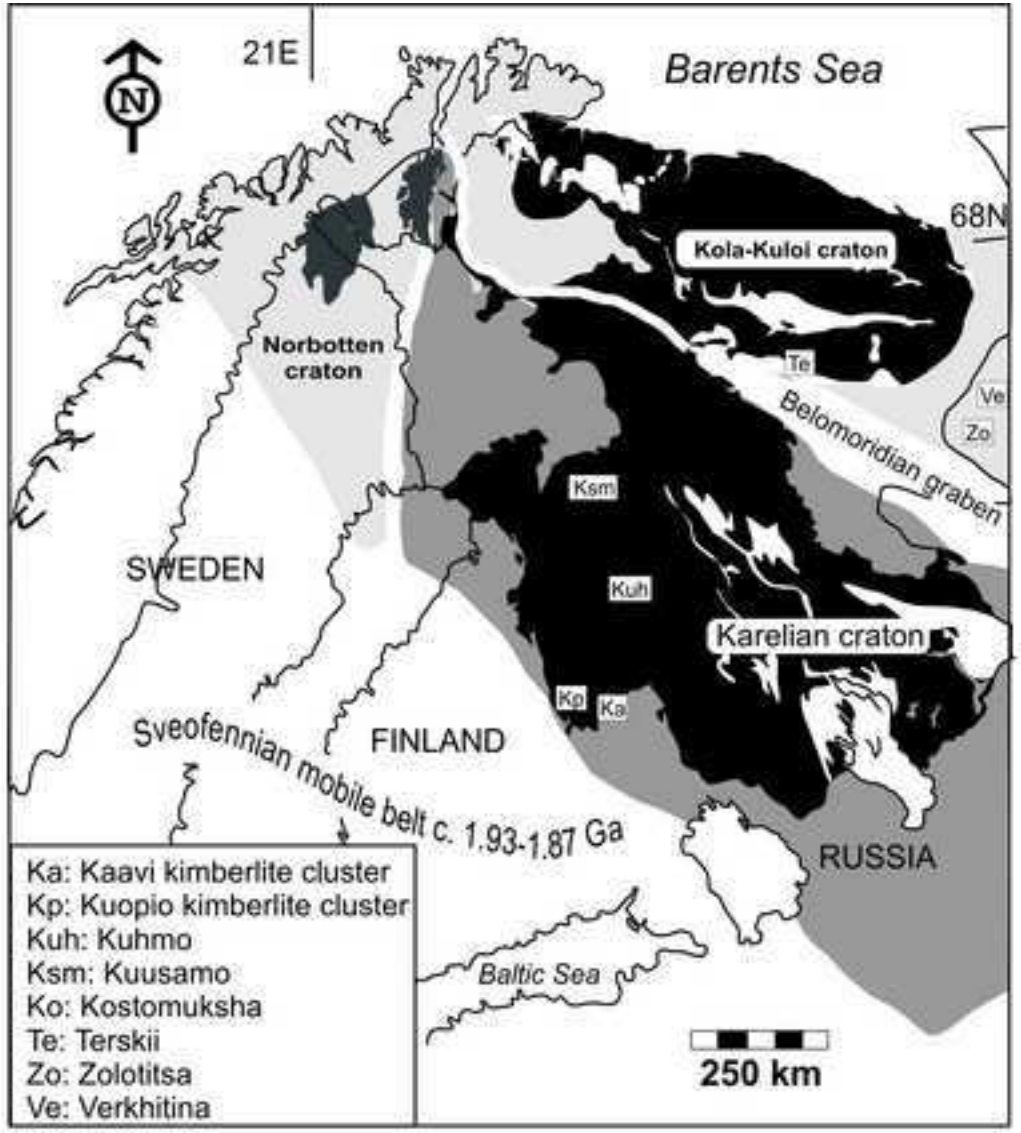

Figure 2

Click here to download high resolution image

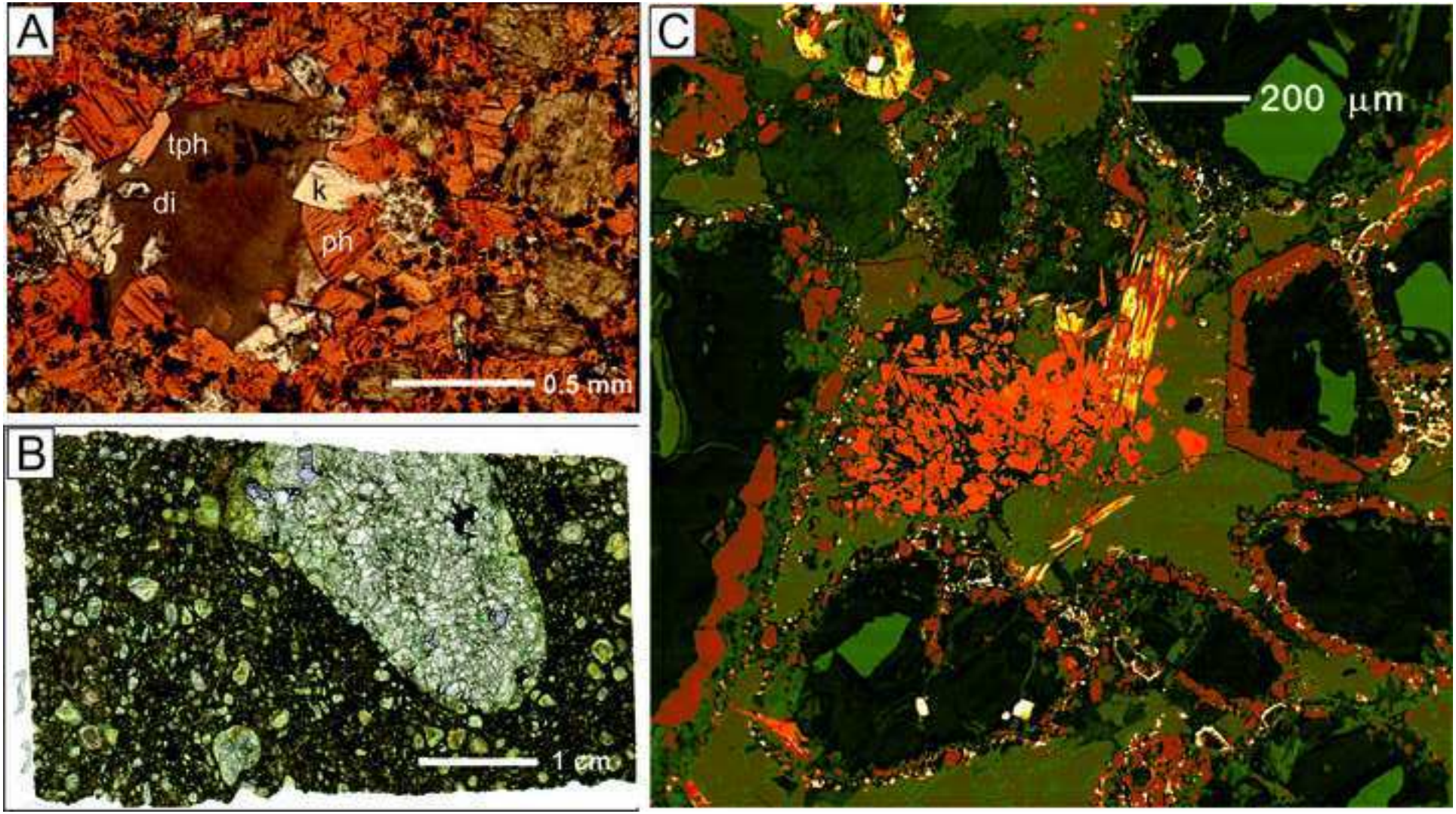

Figure 3

Click here to download high resolution image

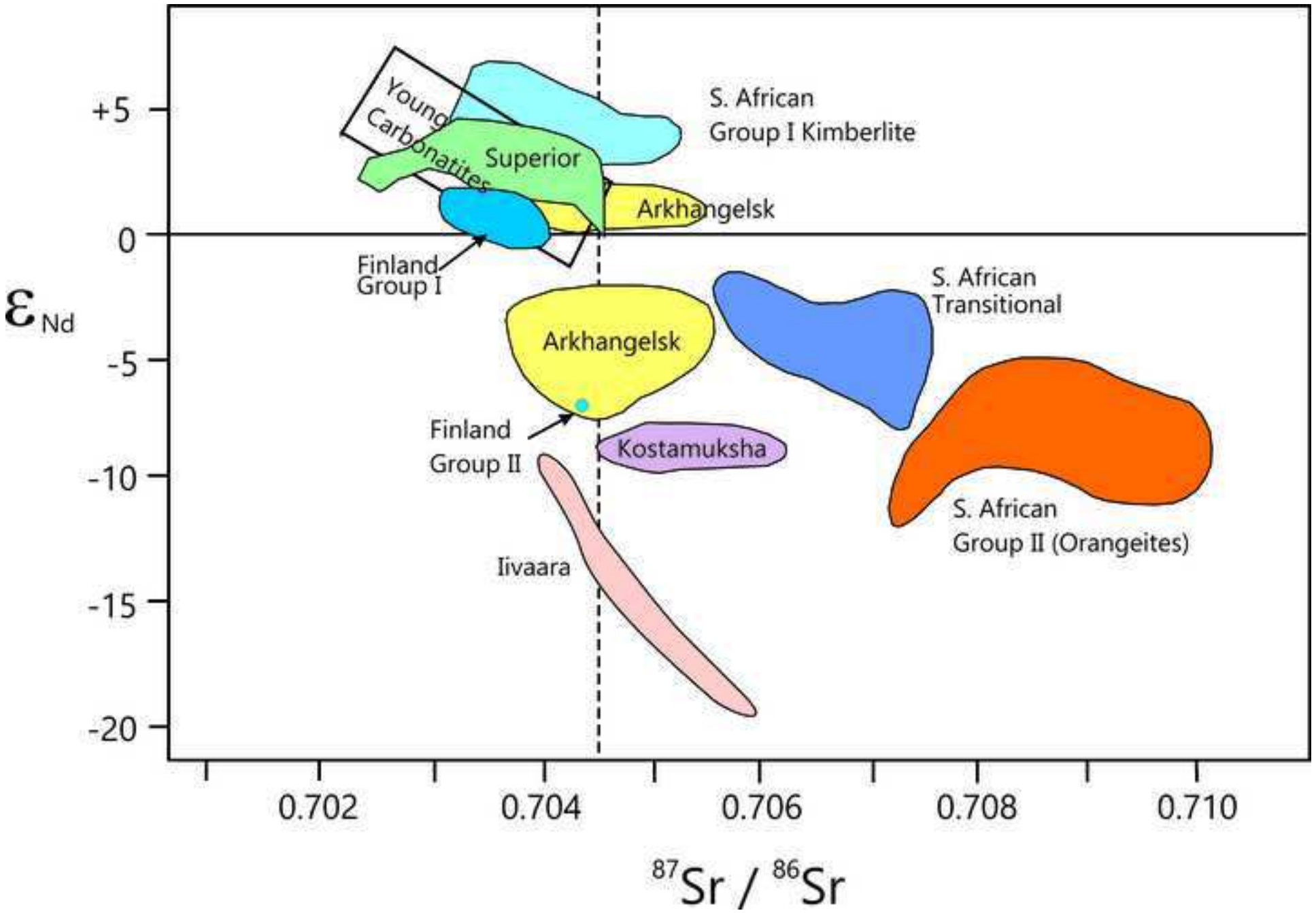

Figure 4

Click here to download high resolution image

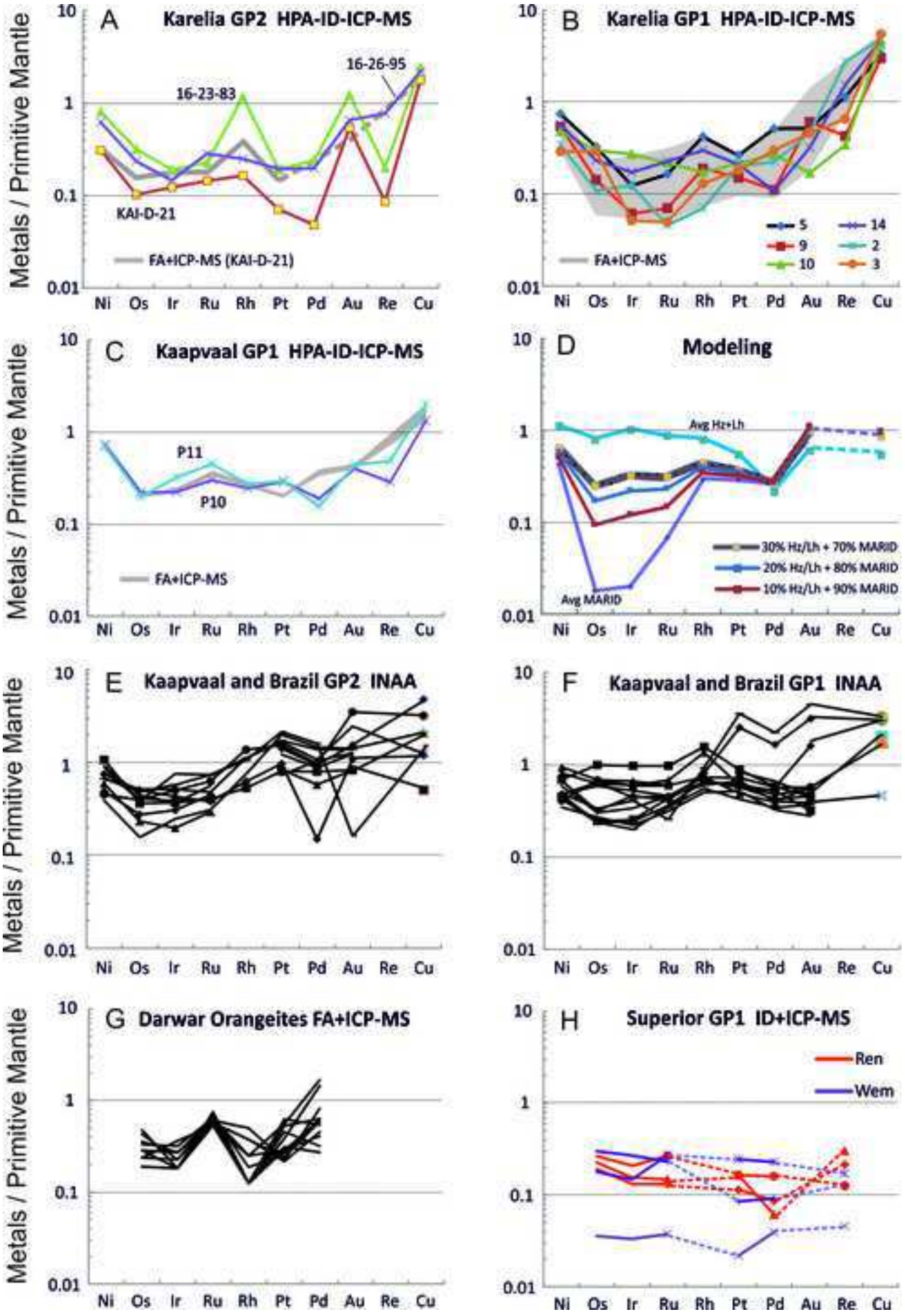

Figure 5
Click here to download high resolution image

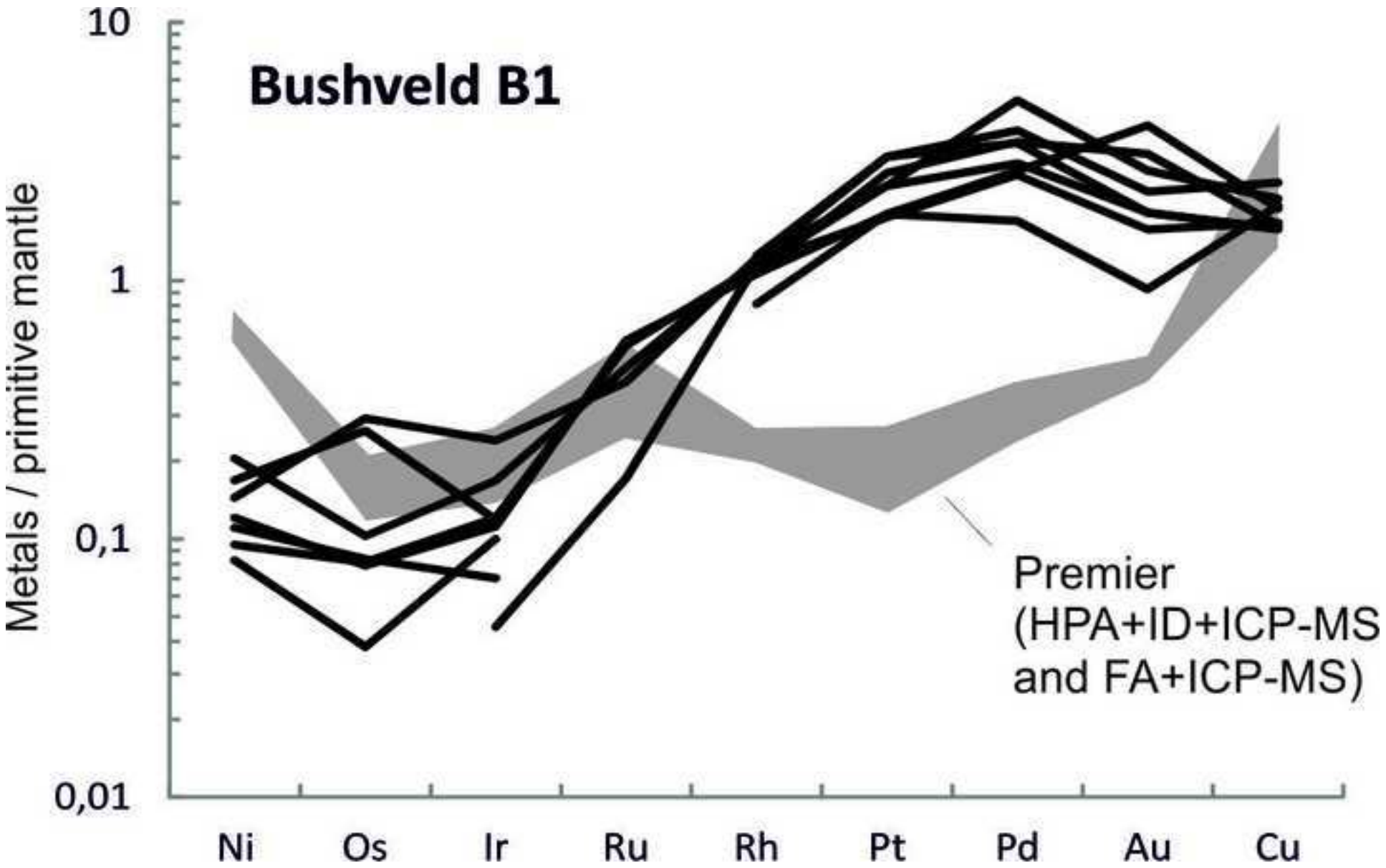

Figure 6

Click here to download high resolution image

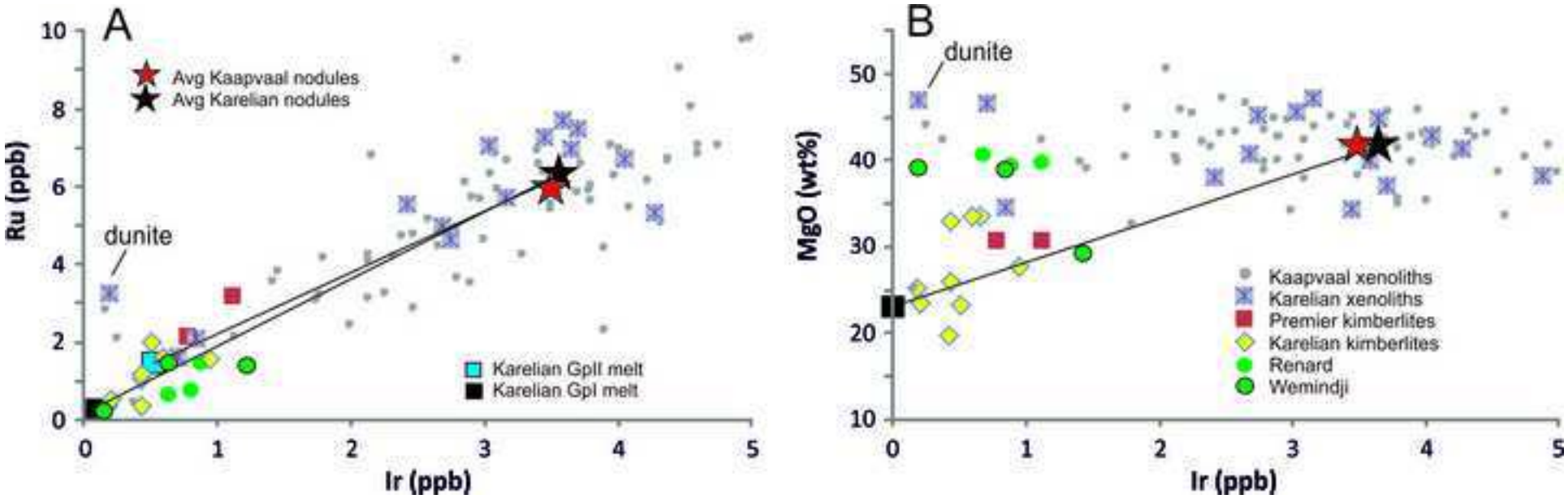

Electronic Annex 1

Click here to download Electronic Annex: Electronic Appendix 1 ICP-MS data of PGE in kimberlites.xlsx

Electronic Annex 2

Click here to download Electronic Annex: Electronic Appendix 2 Modelling table.xls

Manuscript with track changes

Click here to download Source or Other Companion File: Kimberlite paper R2 with track changes.docx